A NEW TYPE OF LIDAR FOR ATMOSPHERIC OPTICAL TURBULENCE

G.G. Gimmestad [(1)], D.W. Roberts [(1)], J.M. Stewart [(1)], J.W. Wood [(1)], M.W. Dawsey[(1)], F.D. Eaton [(2)]

[(1)] GTRI, Georgia Tech, Atlanta, GA USA 30332 E-mail: gary.gimmestad, david.roberts, john.stewart, jack.wood, martha.dawsey, all @gtri.gatech.edu

[(2)] Air Force Directed Energy Directorate, Kirtland AFB, NM USA 87117

ABSTRACT

We are developing a new type of lidar for measuring range profiles of atmospheric optical turbulence. The lidar is based on a measurement concept that is immune to artifacts caused by effects such as vibration or defocus. Four different types of analysis and experiment have all shown that a turbulence lidar built from commercially-available components will attain a demanding set of performance goals. The lidar is currently being built for testing scheduled in August 2006.

1. INTRODUCTION

We are developing a new type of lidar in order to measure range profiles of the strength of atmospheric optical turbulence C_n^2, which is the refractive index structure characteristic. C_n^2 is the variance of the difference in refractive index measured at two points separated by a distance r, divided by $r^{2/3}$. Over the past 25 years, several techniques have been proposed for laser remote sensing of C_n^2 profiles. Most of the techniques were based on efforts to measure the effects of turbulence on a laser beam, such as beam wander or beam broadening. Such techniques are sensitive to instrumental problems, such as defocus or vibrations, which create artifacts that appear exactly the same as the effects of the atmosphere.

In 1998-99, we developed a much better approach based on differential image motion that we call Differential Image Motion (DIM) Lidar and showed that it is free of the artifacts mentioned above [1]. DIM Lidar can be described as a hybrid of two well-established astronomical techniques: the Differential Image Motion Monitor (DIMM), which uses light from natural stars to measure the integrated effect of atmospheric turbulence in terms of Fried's coherence parameter r_0, and laser guide star adaptive optics, in which a laser beam is used to create an artificial beacon at a fixed altitude by focusing the beam and range gating an imager. By moving the guide star through a range of altitudes the DIM profile can be traced out, and an inversion algorithm can retrieve the C_n^2 profile.

The DIM technique measures the variance of the differential wavefront tilt at two spatially-separated apertures. In the focal plane, changes in tilt correspond to image motion, which is why the name of the astronomical instrument incorporates the phrase "differential image motion." This phrase is also incorporated into the name DIM Lidar, and the notation σ_{DIM}^2 is used throughout this paper to mean the DIM variance. Field experiments at Georgia Tech in 1999 using a hard target instead of atmospheric backscatter showed that the technique yields values for path-averaged C_n^2 that are the same as a scintillometer [1]. This was a promising result, but it did not answer the basic questions of how accurately a DIM Lidar can measure $C_n^2(h)$ and with what time and space resolutions. The work described in Sections 3 - 6 of this paper answered these questions. A combination of analysis, field measurements, development and testing of new inversion algorithms, and wave optics simulations was used.

The lidar performance goals are to measure C_n^2 within a factor of two in the range 10^{-18} to 10^{-12} $m^{-2/3}$ from the ground to 10 km altitude, with 10-minute averaging. The DIM Lidar is scheduled for testing against truth data during August 2006.

2. THEORY

Because the DIM LIDAR measures differential wavefront tilt in the same manner as a standard astronomical instrument, much of the analytical model can be adapted from previous work. Eaton [2] presented the first analysis of differential image motion for the DIMM, and we have adapted it for the lidar scenario as

$$\sigma_{DIM}^2 = 33.2(0.349 - 0.242(d/D)^{1/3})D^{-1/3}\overline{C}_n^2, \quad (1)$$

where $\overline{C}_n^2 = \int_0^S C_n^2(s)(1-s/S)^{5/3}ds$ and

σ_{DIM}^2 is the measured DIM variance (radians^2),
S is the distance to the laser beacon,
D is the subaperture diameter (m), and
d is the subaperture separation (m).

3. ANALYSIS

As shown by Eq. 1, σ_{DIM}^2 depends only on the range, turbulence profile, subaperture diameter, and subaperture separation. Morgan [3] showed that centroiding accuracy depends on the image size, the number of photoelectrons in the image, and the numbers of sky background photoelectrons and read-out noise electrons in the image. The image size was calculated by using Gaussian beam theory to find the beam waist diameter at the range of the scattering volume and then modifying it to find the short-exposure image size in the focal plane, based on the turbulence profile along the laser beam path. The numbers of laser and sky photoelectrons in the image were found by using the lidar equation and an equation describing the received power due to sky radiance. Finally, the variance of the image centroid position error was calculated as a function of range. The analysis was performed for a laser wavelength of 355 nm and for atmospheric optical profiles including $C_n^2(h)$, visibility, the scale height, the Angstrom coefficient, the sky radiance, and the lidar ratio.

The DIM Lidar was designed, using commercial components, so that the centroiding error variance will always be small compared to the image motion variance caused by atmospheric turbulence.

In order to optimize the lidar design for anticipated verification tests at the White Sands Missile Range (WSMR) in New Mexico, it was necessary to adopt a set of turbulence profiles that covered a range of conditions, from daytime with a well-developed convective boundary layer to stable nighttime. Three WSMR profiles were adapted from graphs in the IR Handbook [4] a morning profile measured at 0904 MST in the winter, a midday profile, and a night profile. All three were extended to 20 km above sea level with the $HV_{5/7}$ model. The $HV_{5/7}$ model itself was also used as a profile.

The analysis showed that the set of system parameters listed in Tables 1 and 2 is adequate to reach the performance goals, and a lidar with those parameters is currently being built.

Table 1. Transmitter Parameters

Parameter	Value
Laser type	Nd:YAG
Wavelength	355 nm
Pulse Energy	350 mJ
Pulse Repetition Frequency	50 Hz
Pulse Width	3-7 ns
Raw Beam Divergence	650 urad to 1/e^2 intensity level
Raw Beam Diameter	0.7 mm to 1/e^2 intensity level
Output Beam Divergence	15 – 150 urad to 1/e^2 intensity level
Output Beam Diameter at Transmitter	44 mm to 1/e^2 intensity level
Transmitter Aperture Location	Centered on receiver primary mirror behind secondary mirror

Table 2. Receiver Parameters

Parameter	Value
Primary Mirror Diameter	406.4 mm
Secondary Mirror Diameter	152.4 mm
Telescope Prime Focal Length	3414 mm
Telescope Prime Focus Image Scale	3.41 microns per microradian
Prime Focus Diffraction Spot Size	7.3 microns (2.13 urad) at 355 nm
Optical Bandpass	10 nm FWHM centered at 355 nm
System Transmission	25% minimum
Camera Array Format	80 X 80 pixels, 24 um pitch, 100% fill factor
Array Quantum Efficiency	60% at 355 nm
Array Readout Noise per Pixel	4.1 e$^-$ at 50 Hz frame rate and max gain
DIM Aperture Diameters	76.2 mm maximum
Number of DIM Apertures	Four
Aperture Arrangement	Equally spaced on 317.5 mm diameter circle
DIM Channel Effective Focal Length	3414 mm
DIM Channel Image Scale	3.41 microns per microradian

4. FIELD MEASUREMENTS

A set of field measurements was undertaken by using a CW version of the lidar on a tracking mount. Truth data were acquired by raising and lowering micro-thermal probes on a balloon, which also served as a target for the laser beam. The field measurements were interrupted by an accidental release of the balloon and data were acquired only when the atmosphere was rapidly changing, but reasonable agreement between the measured and predicted values of differential image motion was obtained, as shown in Fig. 1. In addition, the scatter in the field test data was shown to agree with the theory presented by Andreas [5, 6] showing that the maximum rate at which we will obtain statistically independent images is about 50 Hz.

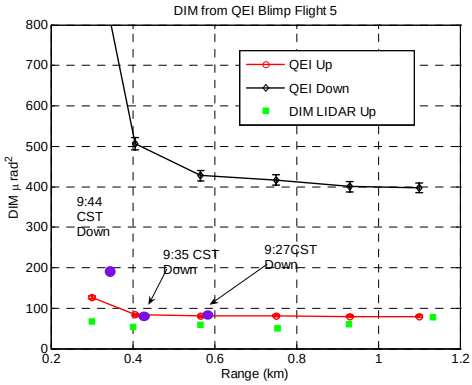

Fig 1. Predicted and measured DIM profiles.

5. INVERSION ALGORITHMS

Eq. (1) can be rewritten as

$$\sigma_{DIM}{}^2(h) = A\int_0^h C_n{}^2(h')(1-h'/h)^{5/3}\,dh' \qquad (2)$$

Where h is the distance from the receiver and A is a constant dependent on geometry of the receiver. Unfortunately, the direct inversion method of finding $C_n^2(h)$ suffers from high noise gain. A graph of the weighting function in the integral of Eq. (2) has a classic shape that always leads to ill-conditioned problems [7]. This means that small uncertainties in the input data, and even the act of discretizing the problem, cause large changes in the output including oscillations and negative values. A more subtle approach is needed. By differentiating Eq. (2), we obtain a very different weighting function that results in a very low noise gain. We refer to this approach as the slope inversion method. Taking the derivative of both sides of Eq. (2) with respect to h we obtain

$$S(h) = \int_0^h C_n{}^2(h')[\tfrac{5}{3}h'(1-h'/h)^{2/3}/h^2]dh'. \quad (3)$$

The weighting functions for the original equation and the slope method are plotted in Fig. 2. Inversion of the new equation is stable, and in addition a set of basis functions was developed that are immune to added noise and to problems such as negative values. Twenty retrievals of the $HV_{5/7}$ profile with random noise added are shown in Fig. 3.

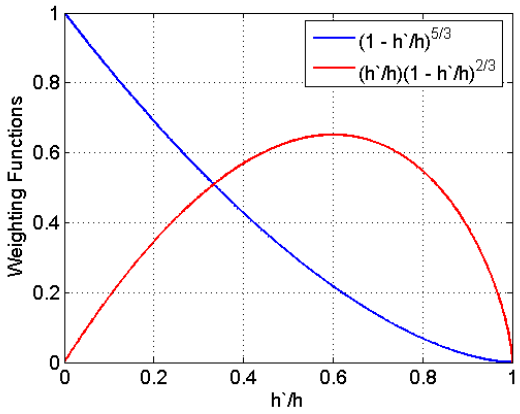

Fig. 2. The weighting functions of the original and the slope method equations.

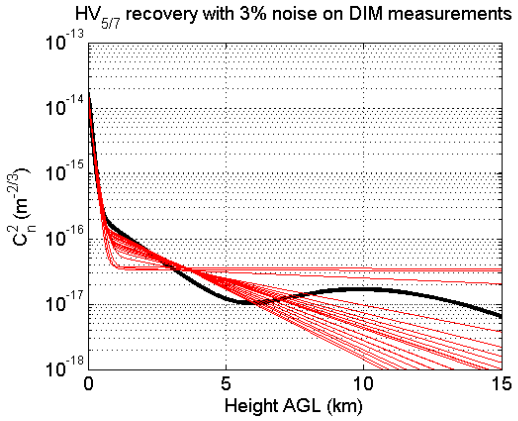

Fig. 3. Retrieval of $HV_{5/7}$ profiles with added noise.

6. WAVE OPTICS SIMULATIONS

The objective of the wave optics simulations was to quantify any errors in the calculations of the system's expected centroiding accuracy caused by approximations in the analysis described above. The Optical Sciences Company (tOSC) did the wave optics simulations under a subcontract.

The system parameters listed in Tables 1 and 2 were used in the wave optics simulations. The laser beam was propagated through turbulence phase screens to each guide star altitude with the beam focused at each altitude. The combination of the laser pulse's inherent intensity distribution and

the distorting effects of the turbulence phase screens determine the resulting guide star intensity distribution. The image of the guide star was found by convolving the turbulence-distorted laser pulse at the guide star altitude with the image of a point source placed at the same altitude. Five thousand centroids were generated for each range and each of the receiver apertures. Differential tilt variances between the subapertures were compared to values produced by using Eq. 1.

Fig. 4 shows the theoretical values of the differential tilt variance along with those generated by the simulation, for the morning profile. All three profiles showed similar agreement between simulation and theory, except at very long ranges where the laser beam diameter becomes comparable to the separation between the subapertures and Eq. (1) no longer describes the geometry correctly.

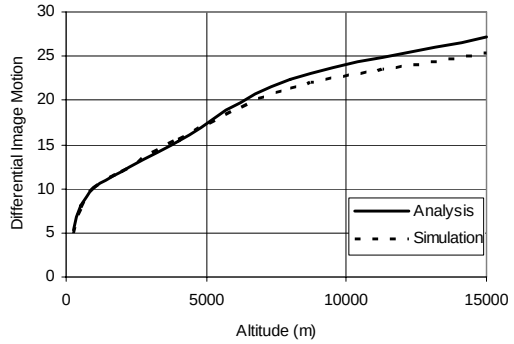

Fig. 4. Comparison of the theoretical and wave-optics simulated differential tilt variances for the morning profile

7. CONCLUSIONS

We are developing a new type of lidar, known as the DIM Lidar, for measuring range profiles of turbulence. An analysis showed that a demanding set of performance goals can be met with a lidar system built from commercially-available components, and the lidar was subsequently designed. Field measurements of DIM were conducted on slant paths through the atmosphere, from the ground to a tethered blimp, with truth data measured by an instrument package carried by the blimp. An analysis of the DIM data showed satisfactory agreement between the measurements and predictions based on Eq. (1). A stable inversion method was developed and a set of well-behaved functions was found to represent DIM.

Finally, wave optics simulations were carried out and the results agreed with the simpler analysis except at the longest ranges. The four research efforts described above all indicate that the DIM Lidar will perform as expected. Tests against truth data are scheduled for August 2006.

ACKNOWLEDGEMENTS

The authors acknowledge the assistance of Mike Jensen at QEI Technologies of Denver, Colorado, Robert Stovall and Rick Welch of the 46th Test Wing at Eglin Air Force Base, Florida, David L. Fried, consultant, Glenn Tyler and Michael Campbell of tOSC, and Ian Gatland, Professor Emeritus in the Physics Department at Georgia Tech. The project is funded under the DTRMC DE T&E/S&T Program. The Executing Agent is Minh Vuong of the U.S. Army PEO-STRI in Orlando, Florida.

REFERENCES

1. M.S. Belen'kii, D.W. Roberts, J.M. Stewart, G.G. Gimmestad, and W.R. Dagle, Experimental validation of the differential image motion lidar concept, *Optics Letters* Vol. 25, 518-520, (2000).

2. F.D. Eaton et al., Comparison of two techniques for determining atmospheric seeing, *Proc. SPIE* Vol. 926, 319-334 (1988).

3. J.S. Morgan, D.C. Slater, J.G. Timothy, and E.B. Jenkins, Centroid Position Measurements and Subpixel Sensitivity Variations with the MAMA Detector, *Applied Optics* Vol. 28, 1178-1192 (1989).

4. F.G. Smith, Ed., *The Infrared and Electro-Optical Systems Handbook* Vol. 2, Atmospheric Propagation of Radiation (1993).

5. E.L. Andreas, Estimating Averaging times for Point and Path-Averaged Measurements of Turbulence Spectra, *J. App. Meteor*. Vol. 27, 295-304 (1988).

6. G.G. Gimmestad, M.W. Dawsey, D.W. Roberts, J.M. Stewart, J.W. Wood, F.D. Eaton, M.L. Jensen, and R.J. Welch, Field validation of optical turbulence lidar technique, *Proc. SPIE* Vol. 5793, 10-16 (2005).

7. S. Twomey, *Introduction to the Mathematics of Inversion in Remote Sensing and Indirect Measurements*, Dover, New York, (1977).